Environmental Science and Pollution Research (2018) 25:8620–8635
https://doi.org/10.1007/s11356-017-1122-8

RESEARCH ARTICLE

DPF soot as an adsorbent for Cu(II), Cd(II), and Cr(VI) compared with commercial activated carbon

Kun Yang[1] · John Fox[1]

Received: 5 July 2017 / Accepted: 21 December 2017 / Published online: 9 January 2018

Abstract

The use of carbon soot recovered from diesel particulate filters (DPF) has been investigated as a potential adsorbent for heavy metals including cadmium, chromium, and copper from wastewater. Results were compared with the adsorption performance of powder activated carbon (PAC). The uptake capacity of heavy metals for soot was found to be higher than PAC. And the thermodynamic study result for both soot and PAC indicated the adsorption procedures are exothermic. The adsorption studies were carried out for both single and binary systems. The data are best modeled by the monolayer model and Langmuir isotherm model for single systems. The adsorption mechanisms are more complex for binary systems. The kinetic studies indicated the adsorption happens rapidly within the first 1 h, and the results can be best modeled by pseudo-second-order model. The SEM-EDS analysis revealed the soot possesses higher porosity and surface area. Carboxylic and hydroxyl functional groups are the predominant surface functional group on both soot and PAC as revealed by FTIR and IEP values. The adsorption can be explained by both Van Der Waals force and electrostatic force.

Keywords DPF soot · PAC · Adsorption · Isotherms · Heavy metal removal

Introduction

Mining, electroplating, metal processing, power generation, textile, and battery manufacturing are the predominant industrial sources of heavy metals, which include Pd, Cd, Cu, Cr, Hg, As, Mg, and Zn, among others (Amarasinghe and Williams 2007; Wang et al. 2011; Zhou et al. 2010; Mishra and Patel 2009). Once these heavy metals are released into the environment, they can accumulate in plants, animals, or drinking water and have the potential to negatively affect the blood system, lungs, kidneys, and the central nervous system in humans (Amarasinghe and Williams 2007; Zhou et al. 2010). Due to the fact that heavy metals can produce both mutagenic and carcinogenic outcomes to humans and aquatic organisms, the United States Environmental Protection Agency (USEPA) has strict regulation controls on heavy metal water pollution (Mohan and Singh 2002; Cho et al. 2011). For example, the maximum contaminant level (MCL) for drinking water enforced by the USEPA is 0.005 mg/L for Cd, 0.1 mg/L for Cr, and 1.3 mg/L for Cu (USEPA. 2009).

Due to the human health risk, numerous technologies have been developed and applied to eliminate heavy metals from aqueous systems. Chemical precipitation followed by coagulation has been employed for the removal of heavy metals at water and wastewater treatment plants, but is not practical for point-of-use application. Ion exchange resin and membrane filtration are both efficient ways to remove heavy metals but ion exchange resin requires complicated water pretreatment, and the fouling problem associated with membranes discourages the use of these technologies (Amarasinghe and Williams 2007; Wang et al. 2011). Other treatment technologies that include oxidation/reduction, dialysis/electrodialysis, and electrolytic extraction are also applied to remove heavy metal or reduce its toxicity (Mohan and Singh 2002). However, those treatment technologies suffer the problem of high cost (Mohan and Singh 2002). Adsorption is a non-selective way to remove organic pollutants and trace amount of heavy metals from water with low cost. The adsorption process is generally considered highly effective, easy to operate, and easy to access (Mohan and Singh 2002).

Responsible editor: Guilherme L. Dotto

✉ John Fox
jtf211@lehigh.edu

[1] Department of Civil and Environmental Engineering, Lehigh University, Bethlehem, PA 18015, USA

Over the past century, numerous adsorbents have been developed in order to treat heavy metals in water. Activated carbon is created by carbonizing organic materials including coconut shells, anthracite coal, bituminous coal, nut shells, and wood. The resultant activated adsorbent is the most widely used due to the large surface area, microporous structure, and affordability (Mohan and Singh 2002). Activated carbon can be widely used in odor removal, de-coloration, gold recovery, mercury removal at coal power plants, and solution purification (Mohan and Singh 2002). However, with regard to heavy metals, commercial activated carbon suffers the problem of low adsorption capacity and selectivity for the heavy metals (Mahvi et al. 2005). For those reasons, many studies have been carried out to develop effective substitutes and low cost adsorbents (Srivastava et al. 1989; Mellah and Chegrouche 1997; Jiang et al. 2010; Rao and Kashifuddin 2016; Okieimen et al., 1991; Cheung et al. 2000). The activated carbon substitute should be easily accessible, economically feasible, and highly effective. Therefore, many naturally occurring materials have been tested for their affinity to remove heavy metals from aqueous systems.

Natural montmorillonite clay was used to remove Pd and Cd from water, with adsorption capacities of 0.68 mg/g for Pb and 0.72 mg/g for Cd (Srivastava et al. 1989). Natural bentonite was found to remove zinc from water with an adsorption capacity of 52.91 mg/g (Mellah and Chegrouche 1997). One study conducted by Jiang et al. (2010) revealed that the adsorption capacity for Pb, Cd, Ni, and Cu from water, on natural kaolinite, was 4 mg/g for Pb, 2.4 mg/g for Ni, 3 mg/g for Cd, and 1.8 mg/g for Cu. The adsorption capacity of Cd-contaminated water was quantified as 27.27 mg/g according to the study using clay balls by Rao and Kashifuddin (2016). Natural peanut husks were appraised to possess Cd adsorption capacity of 0.36 mmol/g and Pb capacity of 0.19 mmol/g (Okieimen et al. 1991). Bone char was applied to remove Cd from water with a maximum adsorption capacity of 0.534 mmol/g as reported by Cheung et al. (2000).

Carbon black is a commercially significant carbonaceous component intentionally produced by the incomplete combustion of an organic precursor such as coal or other fossil fuel (Street et al. 2001). Carbon black is also created as an undesirable by-product of the combustion of coal and fossil fuels, which is a main component of $PM_{2.5}$ (Hamilton and Mansfield 1991). One-year air quality data from an urban site in Finland determined that around 14% of PM $_{2.5}$ was black carbon and more than 90% of the black carbon can be classified as $PM_{2.5}$ (Viidanoja et al. 2002). In this same Finnish study, diesel vehicles were determined to be the major carbon black sources (Viidanoja et al. 2002). This carbon black problem is more severe in other countries, for example China, which has high usage of coal and high density of vehicle use in urban areas (Street et al. 2001). In order to solve this problem, Europe and North American has legislated all the on-road diesel vehicles need to be equipped with a diesel particulate filter (DPF) (Salvat et al. 2000). More than 90% of carbon black or soot as well as the ash can be captured by the DPF (Sappok et al. 2009). As the soot loading increases, the carbon black and ash need to be periodically removed from the DPFs. The loading of soot in a DPF removed for cleaning was measured as 4.5 g of soot per liter of DPF substrate (Yang et al. 2016). In recent efforts, researchers have applied carbon black as an adsorbent to remove heavy metals from aqueous solution (Wang et al. 2011; Zhou et al. 2010; Sappok et al. 2009). The adsorption capacity of commercial carbon black for Cd from water is over 250 mmol/kg and for Cu from water is 400 mmol/kg (Zhou et al. 2010). The Cu, Pb, and Cd maximum adsorption capacity of wheat residue-derived carbon black is higher than 200 mmol/kg (Qiu et al. 2008). Therefore, it is highly desirable to identify alternative sources and alternative generation methods for high efficiency carbon black for heavy metal removal. Among these alternatives, DPF soot was appraised herein as compared to commercially available powdered activated carbon (PAC).

In the present study, soot collected from a commercially used DPF was collected and appraised as a potential adsorbent. The heavy metal adsorption capacity for both DPF soot and PAC were evaluated by bench scale isotherm and kinetic tests. The target pollutants were selected as Cu(II), Cd(II), and Cr(VI). The overall objective of the study was to investigate the adsorption of three heavy metals, Cd(II), Cu(II), and Cr(VI), onto DPF soot in a single and binary system. The first objective of the study determined the adsorption capacity of Cd(II), Cu(II), and Cr(VI) when comparing DPF soot to commercially available activated carbon. The second objective determined the adsorption mechanisms through surface characterization, EDS mapping, and Fourier transform infrared spectroscopy (FTIR).

Table 1 Summary of adsorption isotherms performed during the experiment

Single system			Binary system		
	25 °C	40 °C		25 °C	
	20–200 mg/L			20–200 mg/L	20 mg/L
Cd(II)	√	√	Cd(II)/Cr(VI)	Cd(II)	Cr(VI)
Cr(VI)	√	√	Cr(VI)/Cu(II)	Cr(VI)	Cu(II)
Cu(II)	√	√	Cd(II)/Cu(II)	Cd(II)	Cu(II)

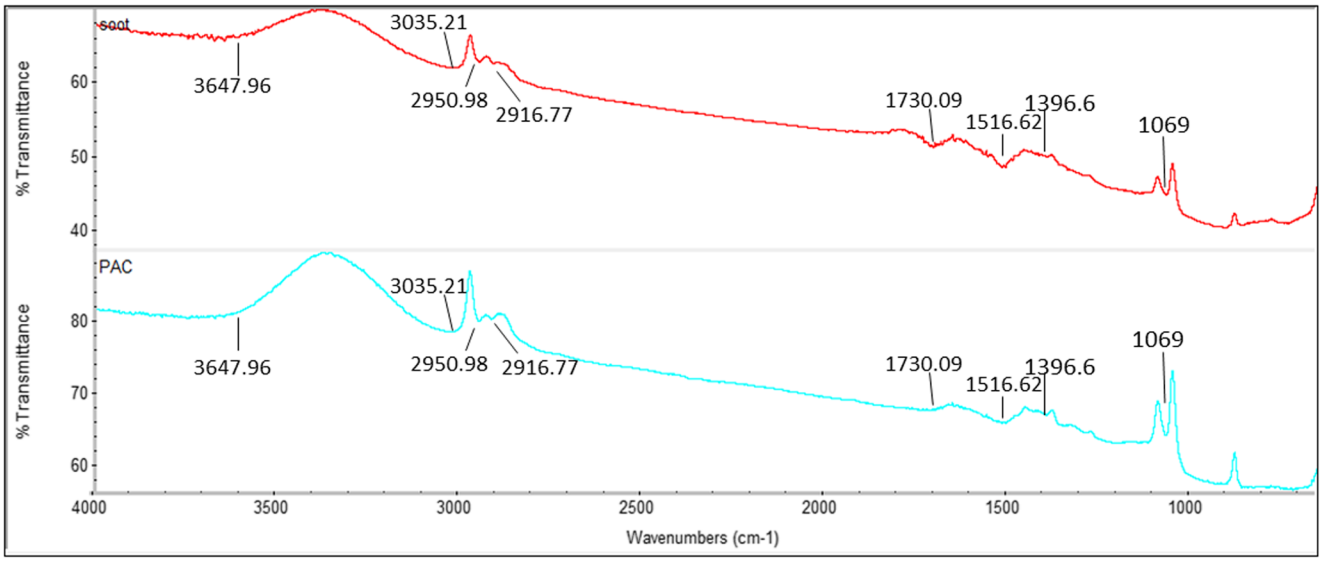

Fig. 1 The Fourier transformed infrared spectra (FTIR) of DPF soot (top) and PAC (bottom)

Material and methods

Preparation of the adsorbents

Soot collected from a diesel particulate filter (DPF) was provided by Hunsicker Emission Services, LLC, whom specializes in DPF regeneration and cleaning. Hunsicker Emission Services, LLC, provided soot which was used for the experiments herein. DPF soot as received contained impurities from lubricating oil additives and metallic ash particles. In order to prepare and purify the soot, 10 g of soot was added to 100 mL of nitric acid (1 M). The slurry of soot and nitric acid was thermally treated under 80 °C for 24 h to remove the diesel ash impurities from the soot. The soot and acid slurry was then passed through a 0.45-μm glass fiber filter, and the soot retained on the filter paper was rinsed with distilled water several times until the solution pH reached 5.0. The soot was dried for 24 h at 105 °C, then was sieved through a No. 200 U.S. Mesh sieve and soot was retained

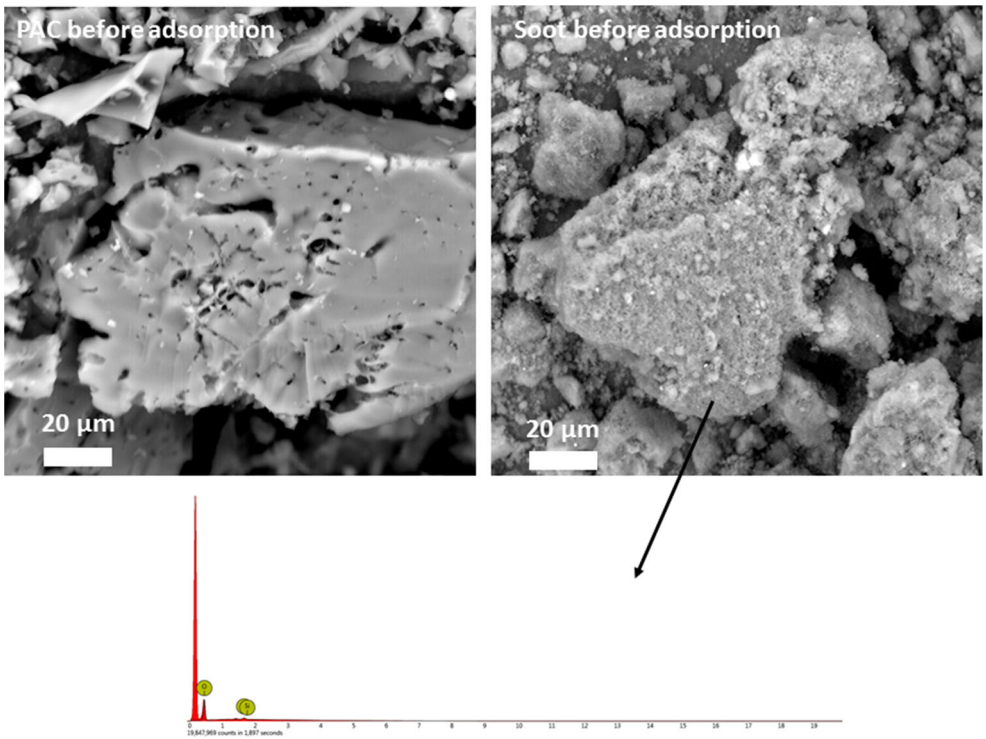

Fig. 2 Surface microstructure of untreated coconut shell PAC before adsorption (left) and soot before adsorption (right), the bottom EDS mapping of soot

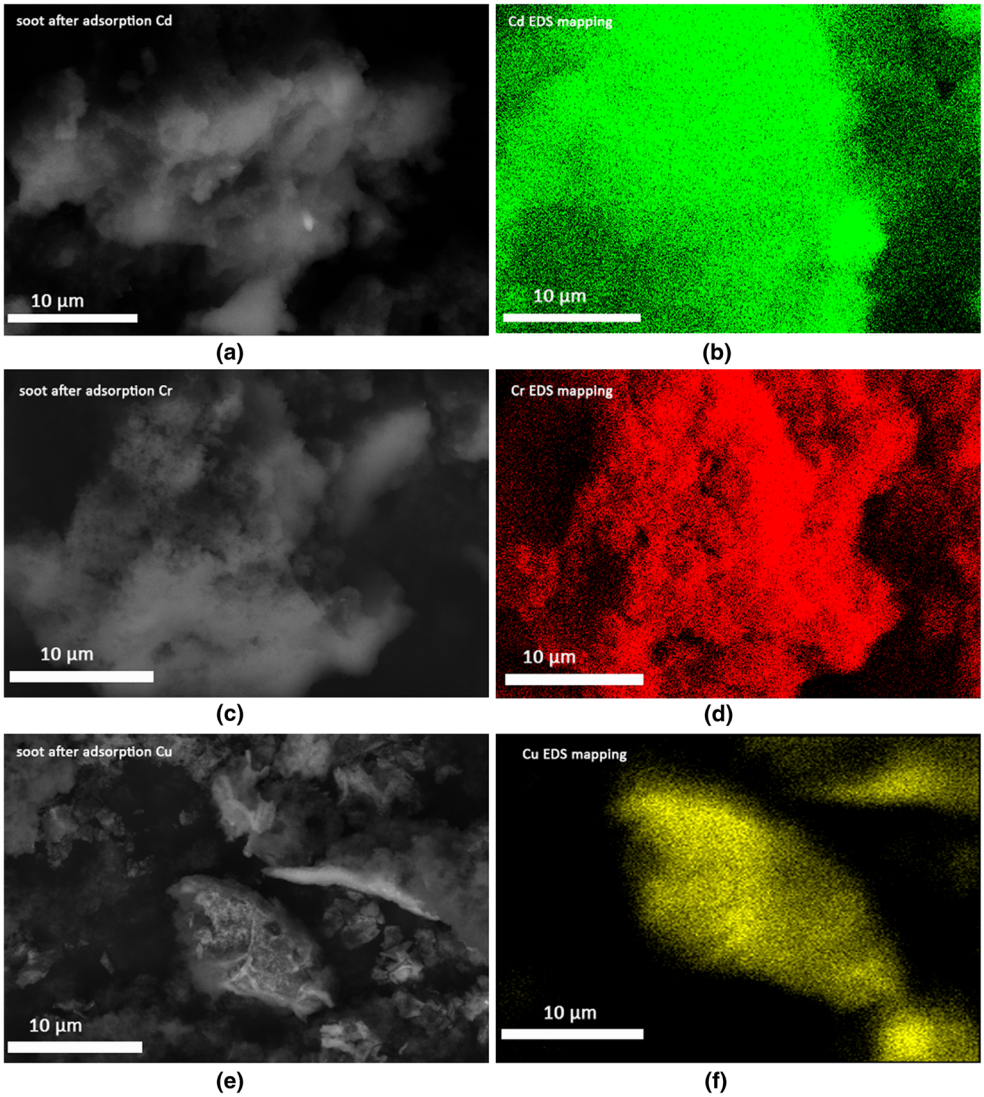

Fig. 3 Elemental mapping of Cd(II), Cr(VI), and Cu(II) on soot (single system at 25 °C): SEM soot (**a**, **c**, **e**), elemental mapping Cd (**b**), Cr (**d**), Cu (**f**)

on No. 325 U.S. Mesh sieve, yielding a purified 200 × 325 DPF soot sample. The soot was rinsed on the No. 325 U.S. Mesh sieve and dried at 105 °C prior to use.

Coconut shell based, unmodified, activated carbon was provide by Evoqua, LLC. The provided granular activated carbon was ground with a Breville coffee grinder (BCG800XL). The ground activated carbon was sieved through a No. 200 U.S. Mesh sieve and was retained on No. 325 U.S. Mesh sieve, yielding a 200 × 325 PAC sample. The PAC was rinsed by distilled water on the No. 325 U.S. Mesh sieve. The PAC was then dried at 105 °C prior to use.

Fourier transform infrared spectroscopy

Infrared spectra (IR) of the DPF soot and powder activated carbon (PAC) were analyzed using a Thermo-Scientific FTIR spectrometer with a deuterated triglycine sulfate detector frequency range of 500–4000 cm^{-1}. Samples were totally dried under oven at 105 °C and prepared as powder to use. Results spectra were compared to the standard FTIR peak table to determine the functional groups detected on the DPF soot and PAC surface.

Measurement of surface zeta potential

The surface zeta potential of DPF soot and PAC under a range of pH conditions were determined by a Malvern Zeta-Sizer. The suspensions were prepared by adding 0.05 g of soot or PAC into 50 ml of deionized water and adjusting the pH to set-points in the range of 1.0 to 10.0. The isoelectric point (IEP) was then determined by plotting the line chart of pH versus zeta potential. The pKa value equals to the IEP. The surface functional groups was determined by finding out the pKa value of the soot and PAC.

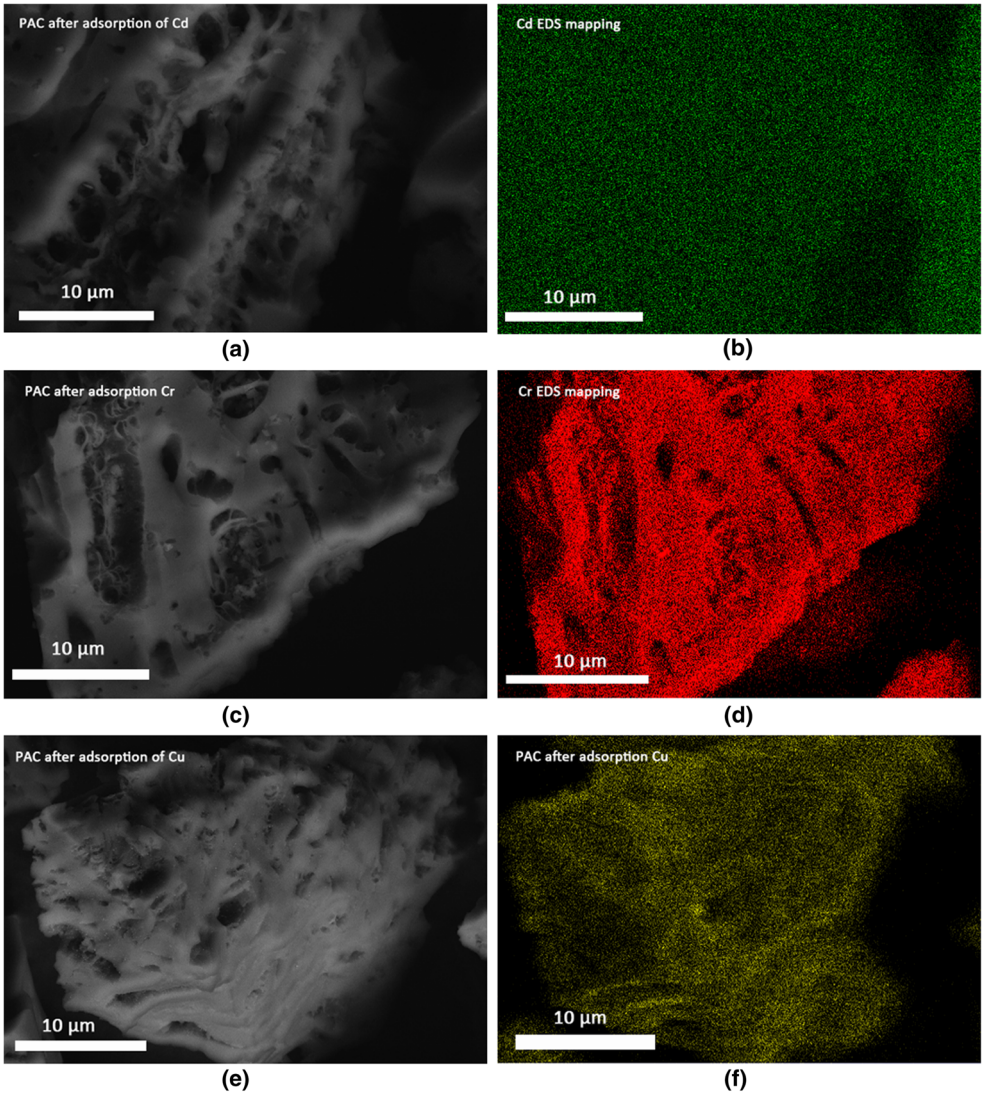

Fig. 4 Elemental mapping of Cd(II), Cr(VI), and Cu(II) on PAC (single system at 25 °C): SEM PAC (**a**, **c**, **e**), elemental mapping of Cd (**b**), Cr (**d**), and Cu (**f**)

Surface characterization of DPF soot and PAC by SEM-EDS

The soot and PAC particles before and after adsorption were dried in an oven for 24 h at 105 °C. The surface microstructure of DPF soot and PAC particles before and after adsorption were analyzed by scanning electron microscopy (SEM) with an accelerating voltage of 15 keV. The elemental map of the DPF soot particles after adsorption of Cr(VI), Cu(II), and Cd(II) were analyzed by electron dispersive spectroscope (EDS).

Synthetic wastewater preparation

Water solutions were prepared by dissolving analytical grade copper nitrate, cadmium acetate, and potassium dichromate in distilled water separately to obtain Cd(II), Cu(II), and Cr(VI) concentrations of 1000 mg/L. During the experiments, the stock solution was diluted to the desired concentration and the pH of the solution was adjusted to 4.5 ± 0.5 by nitric acid and ammonia solution to prevent the precipitation of the target chemicals.

Batch experiments

Batch tests appraising the adsorption isotherms were performed by adding 0.1 g of soot or PAC to 200 mL of prepared solutions to maintain metal concentrations from 20 to 200 mg/L. The mixtures were shaken in a thermostatic shaker (New Brunswick Scientific, Co. Inc.) with a stirring rate of 200 rpm and temperature maintained at 25 °C. The samples were shaken for 24 h, and then removed. The sample was filtered with a 0.45-µm glass fiber filter. The filtrate was analyzed for metal concentration with atomic absorption spectrometry (AAS)

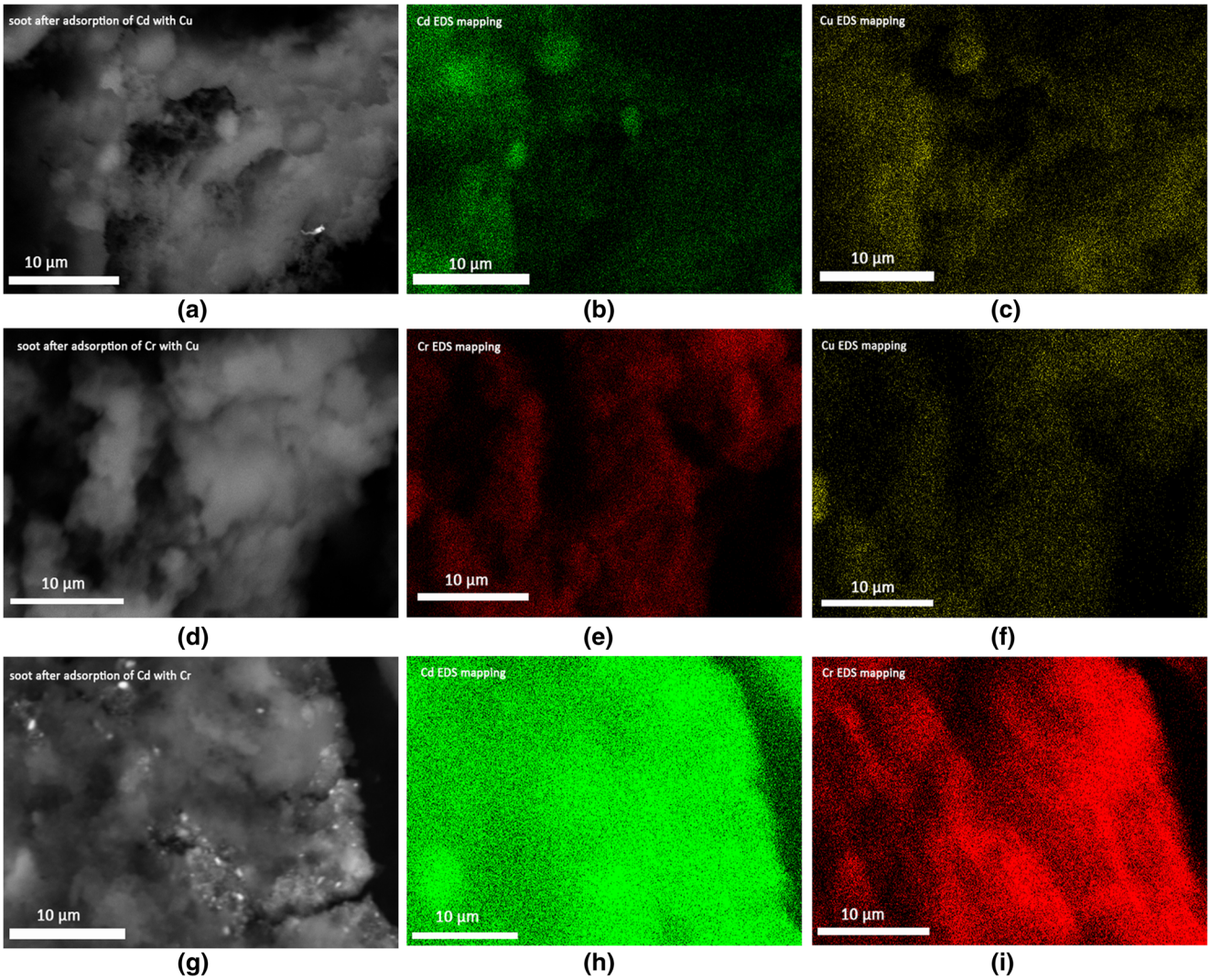

Fig. 5 Elemental mapping of Cd(II)/Cu(II), Cr(VI)/Cu(II), and Cd(II)/Cr(VI) on soot (binary system at 25 °C): SEM soot (**a**, **d**, **g**), elemental mapping of Cd (**b**, **h**), Cu (**c**, **f**), and Cr (**e**, *i*)

(Perkin Elmer AAnalyst 200). In order to determine the effect of temperature and competitive adsorption, the same procedure as described was utilized, but temperature was adjusted from 25 to 40 °C, and dosage concentrations became binary instead of unary. The single compound tests were performed for the three different heavy metals, namely Cd(II), Cu(II), and Cr(VI) with concentrations from 20 to 200 mg/L at 25 and 40 °C. The binary tests were performed by adding Cr(VI) or Cu(II) to Cd(II) or Cr(VI), and Cd(II) to Cr(VI). The experiments were performed with both DPF soot and PAC. The detailed testing matrix is summarized in Table 1:

In order to determine the influence of pH on Cd(II), Cr(VI), and Cu(II) adsorption, tests were performed at a pH of 2.0, 3.0, and 4.0. Specifically, 0.1 g of adsorbent was added to 200 ml of solution with a metal concentration of 160 mg/L. The adsorption capacity (q_e) was compared with respect to pH.

The kinetic studies were carried out by preparing 1.0 L of target solution with a concentration of 100 mg/L of the desired heavy metal. At time zero, 0.5 g of soot or PAC was added to the solution. The mixture was shaken at 25 °C for 24 h with a speed of 200 rpm. At predetermined time intervals, 5 mL samples of solution were withdrawn from the 1.0 L solution. The samples were then filtered with a 0.45-µm glass fiber filter, and the metal concentration was analyzed by atomic absorption spectroscopy (AAS) (Perkin Elmer AAnalyst 200).

Adsorption isotherms

Several equilibrium models have been developed to describe adsorption isotherms. The Langmuir model and Freundlich model are the two most widely used models. The Langmuir isotherm is used to describe the saturated monolayer adsorption over a heterogeneous adsorbent

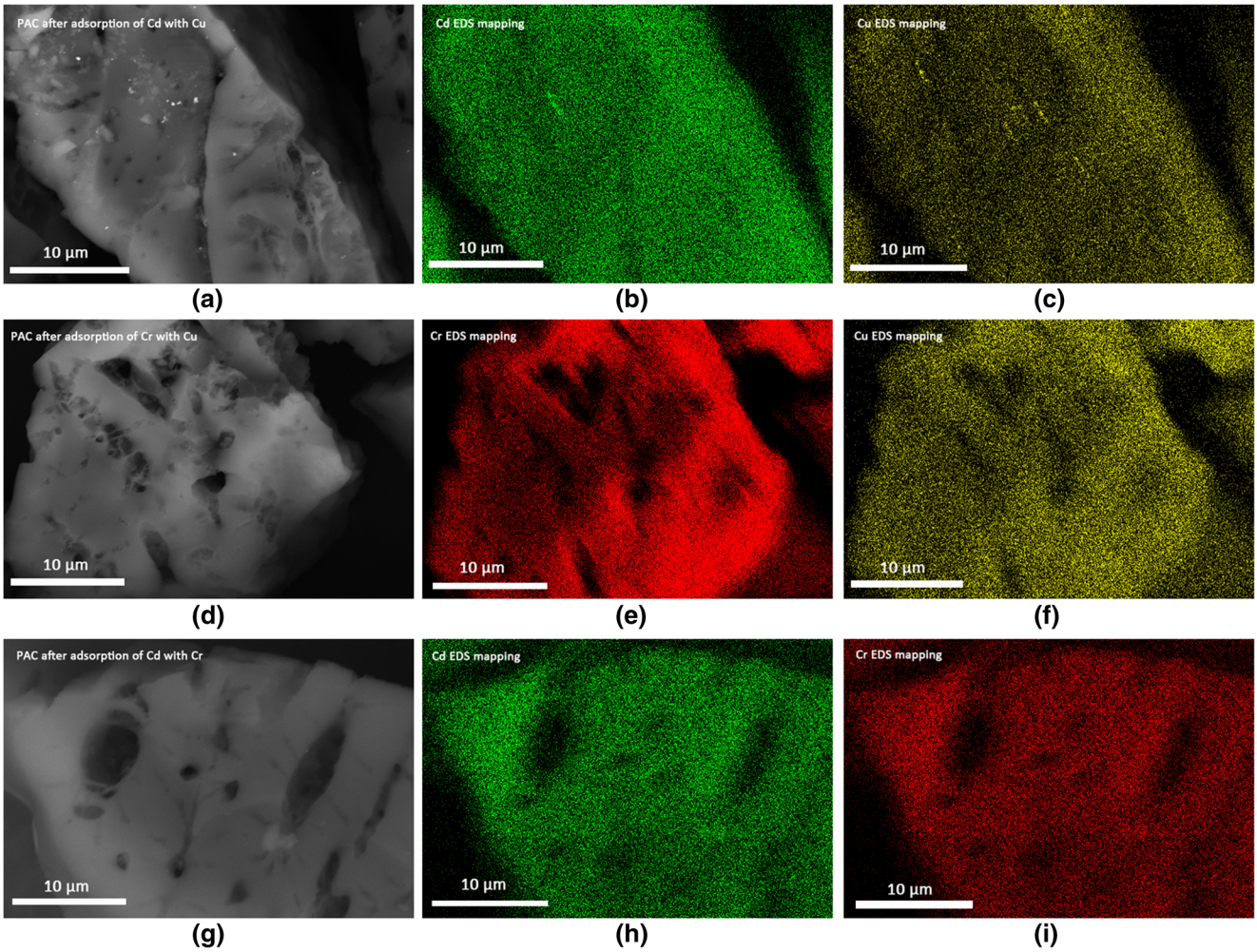

Fig. 6 Elemental mapping of Cd(II)/Cu(II), Cr(VI)/Cu(II), and Cd(II)/Cr(VI) on PAC (binary system at 25 °C): SEM PAC (**a**, **d**, **g**), elemental mapping of Cd (**b**, **h**), Cu (**c**, **f**), and Cr (**e**, **i**)

surface, and the Freundlich isotherm is applied as an empirical, heterogeneous surface adsorption (Mohan and Singh 2002). Additionally, the Langmuir isotherm assumes the adsorption of each molecule onto the surface has the same activation energy while the Freundlich isotherm also suggests that adsorption energy decreases exponentially on completion of the adsorption centers of an adsorbent (Kyzas et al. 2014). In addition to Freundlich and Langmuir, a monolayer model developed by Sellaoui et al. (2017) was also applied during the analysis; it is theoretically based on how a receptor site can accept numerous metal ions which is different from the Langmuir model.

The amount of metal adsorbed by the adsorbents in the system was calculated by the mass balance Eq. 1:

$$q_e = \frac{V(C_0 - C_e)}{m} \tag{1}$$

The Langmuir model, Freundlich model, and monolayer model are described in Eqs. 2, 3, and 4, respectively:

$$q_e = \frac{q_{max} b C_e}{1 + b C_e} \tag{2}$$

$$q_e = K_F C_e^{1/n} \tag{3}$$

$$q_e = \frac{Q_0}{1 + \left(\frac{C_{0.5}}{C_e}\right)^n} \tag{4}$$

where q_e (mg/g) represents the metal concentration retained on the adsorbents, C_0 and C_e are the initial and equilibrium metal concentrations. With regard to the monolayer model, Q_0 is the adsorbed quantity obtained at saturation and n is the number of ions per adsorption site. $C_{0.5}$ stands for the concentration at half saturation. V is the volume of the solution which is 200 ml in the present study and m is the weight of the adsorbent, which is 0.1 g herein.

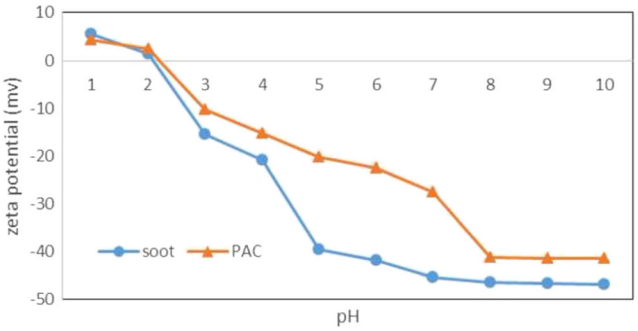

Fig. 7 The surface zeta potential of DPF soot and PAC with variable pH

Adsorption kinetics

Batch tests were performed to determine the kinetics of adsorption. Adsorption kinetics may be controlled by several theories: (1) bulk diffusion, (2) film diffusion, (3) chemisorption, and (4) intra-particle diffusion. (Kyzas et al. 2014). Two commonly applied kinetic models include pseudo-first-order and pseudo-second-order; both were used to analyze the kinetic results herein. The pseudo-first-order model was applied when the initial solution concentration is very high and one adsorbate only occupied one binding site (Kyzas et al. 2014; Azizian 2004). Additionally, pseudo-second-order model implies that one adsorbate species occupied two binding sites due to the chemisorption and when the initial solution concentration is not very high (Kyzas et al. 2014; Azizian 2004). These kinetic rate equations can be written as follows:

$$\ln(q_e - q_t) = \ln q_e - k_1 t \tag{5}$$

$$\frac{t}{q_t} = \frac{1}{k_2 q_e^2} + \frac{t}{q_e} \tag{6}$$

where q_t (mg/g) is the amount of sorbate adsorbed at time t and q_e (mg/g) is the amount adsorbed at time of equilibrium. The k_1 (min) and k_2 (g/mg min) are the rate constants of the pseudo-first-order and pseudo-second-order equation, respectively.

Results and discussions

Fourier transform infrared spectroscopy results

The FTIR spectra in Fig. 1 depict the DPF soot and PAC response. Compared with PAC, the DPF soot particles exhibits the same characteristic peaks. However, the peak position at 1730.09 and 1516.62 cm^{-1}, which stands for C=O stretch in carboxylic acid, are sharper compared to PAC. The peaks at 3035.21, 2950.98, and 2916.77 cm^{-1} represent hydroxyl stretch (-OH) which are very plentiful on the surface of both PAC and soot (Larkin 2011). The plentiful amount of hydroxyl and carboxyl functional groups could interact with the heavy metal cationic ions through electrostatic force. In addition, the soot surface maintains a higher concentration of carboxylic functional groups than PAC as the peaks are sharper (Fig. 1).

Surface characterization of soot and PAC by SEM-EDS

The surface microstructure of DPF soot and PAC before and after the heavy metal adsorption was characterized by SEM, and the surface elemental distribution was analyzed by EDS. The results are shown in Figs. 2, 3, 4, 5 and 6. When compared to PAC, which shows a very smooth surface with some pores evenly distributed throughout, the DPF soot particle surface shows a high degree of roughness as the single carbon black nucleus agglomerate together to form the relatively complicated structures (Fig. 2). The higher surface roughness provides support that the soot obtains larger external surface area and suggests that more adsorption sites are readily available.

The EDS spectra of the DPF soot particle before adsorption demonstrated that the majority of the soot particle is composed of carbon (the highest peak) and oxygen, with trace levels of silicon (Fig. 2). The trace level of silicon might be derived from additives used in lubricating oil in diesel engines (Sappok et al. 2009).

Figures 3 to 6 show the microstructure and elemental distribution of soot particles after adsorption of Cu(II), Cd(II), and Cr(VI) for both single and binary adsorbate systems. The green, red, and yellow represent the

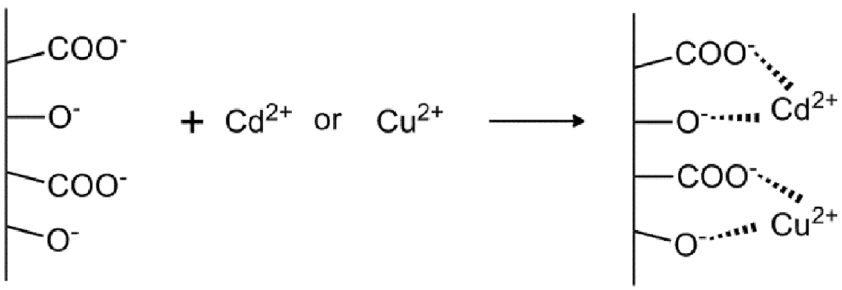

Fig. 8 The adsorption mechanism of Cd(II) and Cu(II)

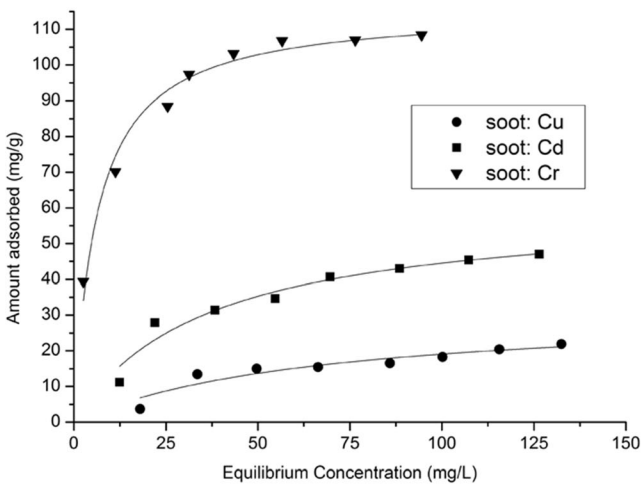

(a) DPF soot Langmuir

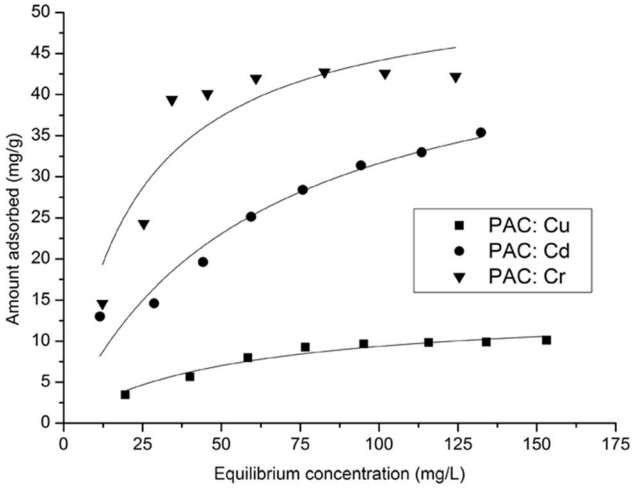

(b) DPF soot Freundlich

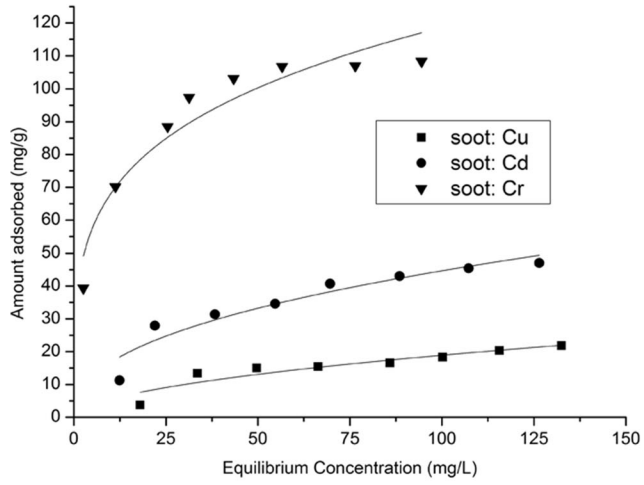

(c) PAC Langmuir

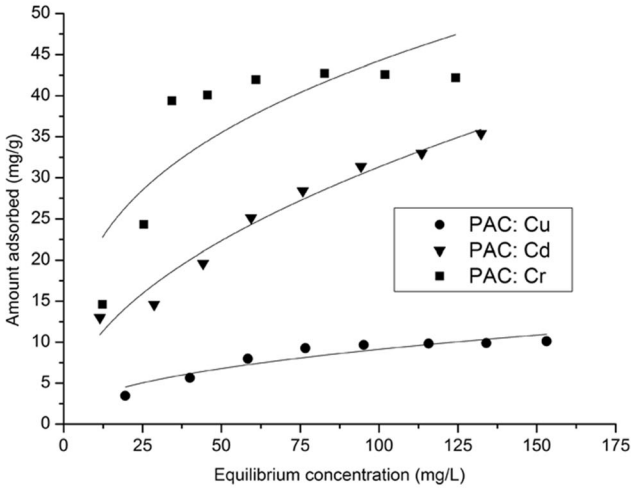

(d) PAC Freundlich

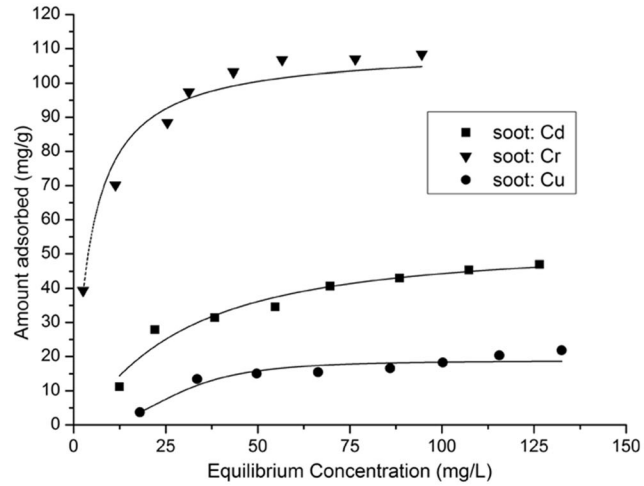

(e) soot Monolayer model

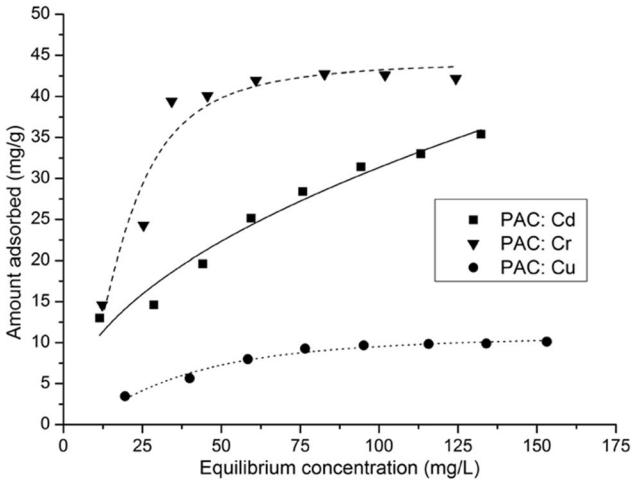

(f) PAC Monolayer model

Fig. 9 Adsorption isotherms of Cd, Cr, and Cu at 25 °C: **a** DPF soot Langmuir, **b** DPF soot Freundlich, **c**, PAC Langmuir, **d** PAC Freundlich, **e** DPF soot monolayer model, and **f** PAC monolayer model

Table 2 Cd(II) and Cu(II) adsorption capacity (mg/g) under variable pH at 25 °C corresponding to initial concentration of 160 ± 20 mg/L

DPF soot			PAC		
pH	Cd	Cu	pH	Cd	Cu
2	22.4	12.1	2	12.4	5.9
3	35.2	13	3	15.7	10.1
4	51.1	25	4	33.1	13

concentration of Cd(II), Cr(VI), and Cu(II), respectively. For all three EDS figures, the soot surface demonstrates much higher Cu(II), Cd(II), and Cr(VI) concentrations compared to the background image. The metals adsorbed on the soot and PAC covered the adsorbent surface as shown in the EDS mapping (Fig. 3–6). The EDS mapping of the binary adsorbate systems in Figs. 5 and 6 show that the competitive adsorption for both soot and PAC lessens the intensity of the single adsorbate adsorption on the surface. Therefore, in the binary system, the existence of two heavy metals reduces the adsorption capacity of the competing heavy metal. The results of the binary system isotherms in Fig. 11 confirmed the EDS mapping results and is in consistence with Sellaoui et al. (2017) that suggests competitive adsorption reduces both Zn and Cd adsorption efficiency.

Surface zeta potential analysis

Figure 7 depicts the effect of pH on the zeta potential of DPF soot and PAC. The zeta potential of both adsorbents became more negative with increasing pH. The isoelectric point (IEP) is defined as the point when the positive zeta potential shifts to negative and is often used to characterize the electro-kinetic behavior of solid surfaces (Strelko et al. 2002). The IEP point can be used to determine the pKa value of surface functional groups. As shown in Fig. 7, the IEP value is between 2 and 3, which corresponds to the pKa value of carboxylic acid. The IEP value for the DPF soot particle is lower, which indicates the degree of surface oxidation increases. Therefore, both the DPF soot and PAC surface shows ample carboxylic functional groups, as confirmed by the FTIR results. As the adsorption solution pH is in the range of 4 to 5, the carboxylic and hydroxyl functional groups loses one hydrogen ion so therefore exhibits a negative charge. The strong carboxylic surface groups are likely responsible for the steep fall in zeta potential (Strelko et al. 2002). According to the following mechanism shown in Fig. 8, the negative charged carboxylic and hydroxyl functional groups have an extremely high affinity for Cd(II) and Cu(II). However, for chromate, the negatively charged functional groups will likely repel each other. Therefore, the chromate adsorption is more likely a result of physical adsorption or can be explained by redox reaction created by the interaction between DPF soot and Cr(VI) (Wang et al. 2010).

Adsorption isotherms

Adsorption isotherm at 25 °C

The adsorption isotherms of Cd(II), Cr(VI), and Cu(II) for soot and PAC at 25 °C are provided in Fig. 9. The results indicate that both DPF soot and PAC have much higher affinity for Cr(VI), followed by Cd(II) and Cu(II). Compared with Cu(II) and Cd(II), the Cr(VI) adsorption behavior is more likely attributed to physical adsorption including Van Der Waals force. Work performed by Wang (2010) suggests that the Cr(VI) can be reduced to Cr(III) by the interaction between carboxylic or hydroxyl acid functional groups on carbon black, and the Cr(III) with three positive charges has extremely high affinity for carbon black (Wang et al. 2010). Since the DPF soot possesses the same surface functional groups as PAC, the interaction between Cr(III) and DPF soot might also induce a similar mechanism. Considering the adsorption of Cd(II) and Cu(II), despite the Van Der Waals force, the

Table 3 Cd(II), Cu(II), and Cr(VI) 25 °C isotherm parameters

	Langmuir			Freundlich			Monolayer model			
Soot	q	b	R^2	k	n	R^2	Q_0	n	$C_{0.5}$	R^2
Cd	86.95	0.0132	0.913	3.92	1.8597	0.857	52.93	2.256	27.2	0.98
Cr	109.89	0.2106	0.987	32.9	3.4722	0.944	126.4	3	7.634	0.987
Cu	82.43	0.0002	0.873	1.5	1.364	0.794	22	2.77	33.524	0.99
PAC	q	b	R^2	k	n	R^2	Q_0	n	$C_{0.5}$	R^2
Cd	32.89	0.051	0.942	3.78	2.1939	0.911	36.8	1.888	21.3	0.945
Cr	69.44	0.0225	0.941	6.11	2.2614	0.767	64.25	2.19	18.46	0.92
Cu	16.42	0.0137	0.986	0.81	1.8903	0.916	16.7	1.86	34.256	0.98

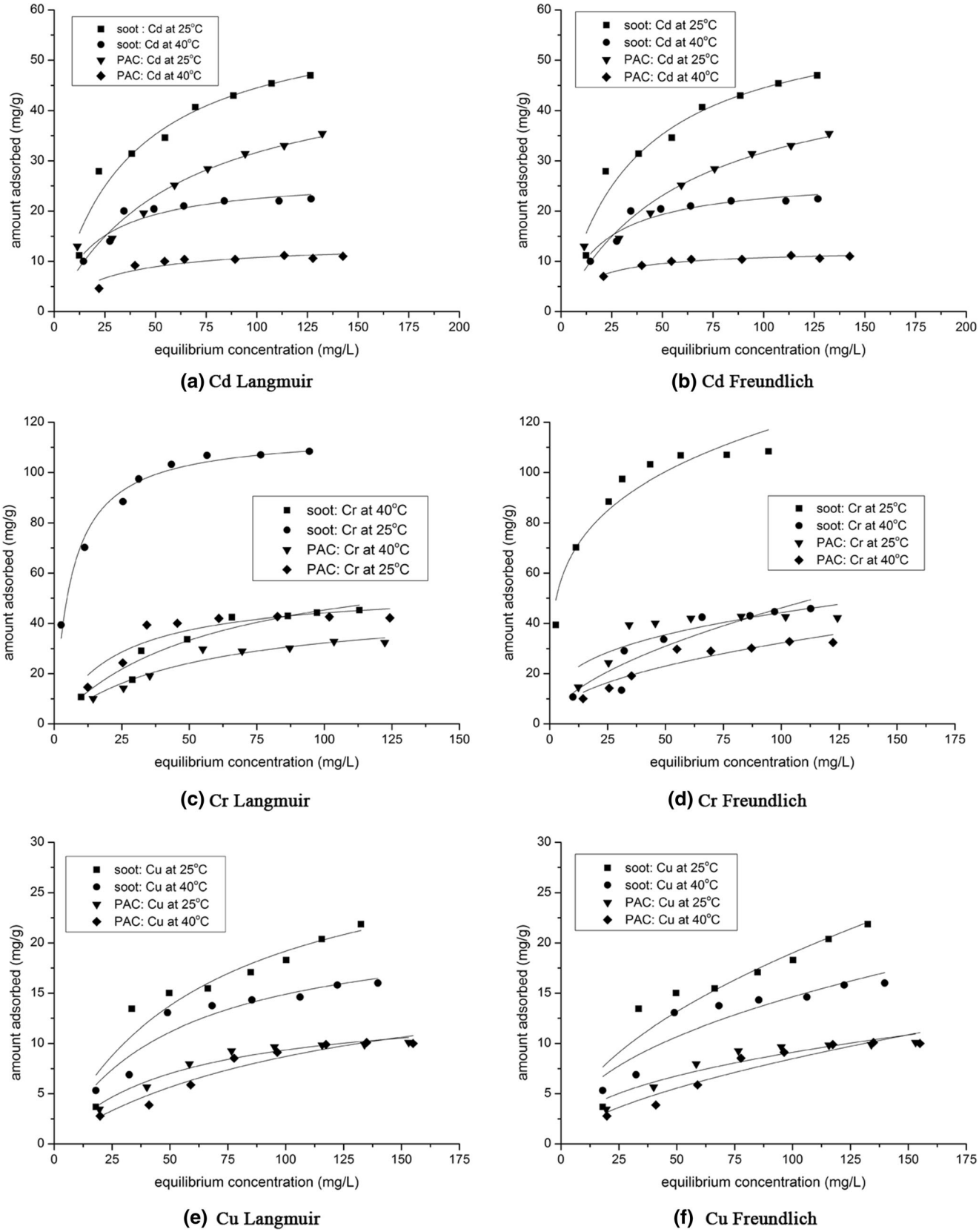

Fig. 10 Effect of temperature on the adsorption isotherms of Cd(II), Cr(VI), and Cu(II): **a** Cd Langmuir, **b** Cd Freundlich, **c** Cr Langmuir, **d** Cr Freundlich, **e** Cu Langmuir, and **f** Cu Freundlich

Table 4 Thermodynamic parameters for the adsorption of Cd(II), Cu(II), and Cr(VI) on DPF soot and PAC

Soot	ΔG(KJ/mol)		ΔH(kJ/mol)	PAC	ΔG(KJ/mol)		ΔH(kJ/mol)
	25 °C	40 °C			25 °C	40 °C	
Cd(II)	− 6.4	− 9.33	− 52.01	Cd(II)	− 9.54	− 10.78	− 10.92
Cu(II)	3.98	− 3.6	− 156.15	Cu(II)	− 5.24	− 5.6	− 3.43
Cr(VI)	− 13.25	− 7.9	− 2.41	Cr(VI)	− 7.71	− 7.15	− 2.29

electrostatic interaction between surface functional groups and cationic ions would facilitate the adsorption as indicated in Fig. 8. In order to figure out the contribution of the electrostatic and non-electrostatic adsorption, adsorption capacity at 160 ± 20 mg/L under elevated pH was presented in Table 2. The degree of dissociation of carboxylic and hydroxyl functional groups increases with increasing system pH, so that pH will impact the surface charge of soot and PAC particles (Zhou et al. 2016). As the pH increased from 2.0 to 4.0, the adsorption capacity increased by almost half for both DPF soot and

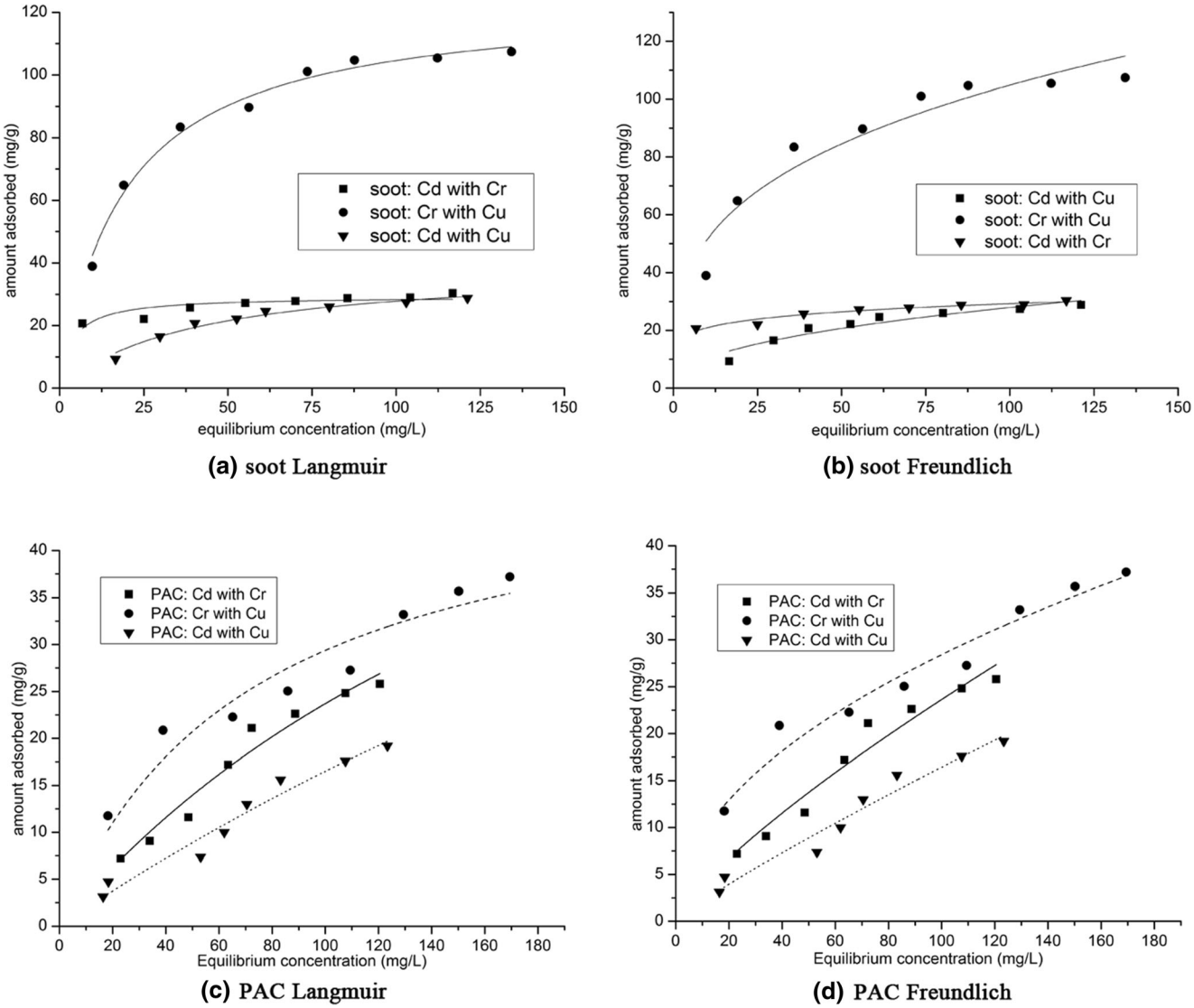

Fig. 11 Binary adsorption of Cd(II), Cr(VI) at 25 °C: **a** soot Langmuir, **b** soot Freundlich, **c** PAC Langmuir, and **d** PAC Freundlich

Table 5 Langmuir and Freundlich isotherm constants for Cd(II), Cu(II), and Cr(VI) adsorption at 40 °C

	Langmuir			Freundlich		
Soot	q	b	R^2	k	n	R^2
Cd	29.76	0.0361	0.936	4.67	2.8802	0.794
Cr	58.82	0.0210	0.872	2.27	1.5221	0.842
Cu	51.28	0.0041	0.979	0.41	1.2822	0.891
PAC	q	b	R^2	k	n	R^2
Cd	12.50	0.0630	0.967	3.99	4.6838	0.846
Cr	53.76	0.0156	0.981	2.32	1.7271	0.932
Cu	18.15	0.0086	0.949	0.340	1.4314	0.946

PAC. According to the zeta potential results, the pH increase from 2.0 to 4.0 results in a deprotonation of carboxylic and hydroxyl functional groups, further facilitating the electrostatic interaction.

The equilibrium adsorption data were modeled with Langmuir, Freundlich, and monolayer isotherms, and the corresponding isotherm constants are in Table 3. It is readily apparent that both Langmuir and monolayer isotherm possesses a higher regression coefficient than the Freundlich isotherm for all the three metals tested herein. These results suggest that the adsorption occurs at discrete adsorption sites on the surface and the maximum adsorption occurs when the surface is covered by a monolayer of adsorbate (Amarasinghe and Williams 2007; Veli and Alyuz 2007). Furthermore, the monolayer model provides the best fit to the data compared with the Langmuir model for all metals tested. The monolayer model was developed based on the Langmuir model but it assumes the single adsorption site can accommodate multiple ions, which is shown as n in the model (Sellaoui et al. 2017). From Table 3, we observe that n(Cr) > n(Cu) and n(Cd), which means that both the DPF soot and PAC are more selective for Cr(VI) than Cu(II) and Cd(II). Therefore, the sorption of Cd(II), Cu(II), and Cr(VI) is most likely occurring at functional groups/binding sites on the surface of the DPF soot and PAC. Therefore, the monolayer model offers better modeling of the adsorption mechanism (Sari and Tuzen 2009; Sellaoui et al. 2017).

Table 6 Langmuir and Freundlich isotherm constants for binary adsorption at 25 °C

	Langmuir			Freundlich		
Soot	q	b	R^2	k	n	R^2
Cd, Cr	51.02	0.0141	0.972	2.51	1.8786	0.903
Cr, Cu	88.91	0.0206	0.999	19.86	2.7285	0.918
Cd, Cu	28.65	0.3431	0.737	15.22	7.0921	0.931
PAC	q	b	R^2	k	n	R^2
Cd, Cr	54.05	0.006	0.907	0.56	1.243	0.900
Cr, Cu	48.70	0.0186	0.939	2.07	2.0631	0.927
Cd, Cu	32.05	0.0075	0.906	0.35	1.2310	0.922

Table 7 Ultimate loading of single and binary systems under 25 °C

Soot	Ultimate loading (mg/g)	Soot	Ultimate loading (mg/g)
Cd	47.0	Cd/Cr	28.8
Cr	108.0	Cr/Cu	107.4
–	–	Cd/Cu	30.4
PAC	Ultimate loading (mg/g)	PAC	Ultimate loading (mg/g)
Cd	35.4	Cd/Cr	25.8
Cr	42.2	Cr/Cu	37.2
–	–	Cd/Cu	19.2

When comparing the ultimate loading of the results in Table 7 for both DPF soot and PAC, it is apparent that the DPF soot possesses higher capacity for Cr (IV) than PAC. Specifically, the DPF soot adsorbed 105 mg Cr (IV) per gram of DPF soot, compared to the 42 mg Cr (IV) per gram of PAC. The ultimate loading for Cd (II) is similar for both DPF soot and PAC. The ultimate loading for Cu (II) is the lowest of all metals tested herein, but is nearly double for DPF soot than that of PAC.

Effect of adsorption temperature

The effect of temperature on the adsorption capacity was studied at 25 and 40 °C, and the results are presented in Fig. 10 and Table 5. The adsorption capacity decreased as the temperature increased from 25 to 40 °C for all three metals. As previously reported, the Langmuir isotherm provides the best fit for both 25 and 40 °C, which means that the temperature change does not alter the adsorption mechanism and adsorption sites on the DPF soot and PAC (Table 4). In order to confirm the results that the adsorption process is an exothermic reaction, the Gibbs' free energy (ΔG) and enthalphy (ΔH) were calculated using Eqs. 7 and 8:

$$\Delta G^0 = -RTln(K_1) \tag{7}$$

$$\Delta H^0 = -R\left(\frac{T_2 T_1}{T_2 - T_1}\right)\ln\left(\frac{K_2}{K_1}\right) \tag{8}$$

where K_1 and K_2 are the Langmuir constants, b, from Table 3 multiplied by 1000, corresponding to the b values at both 25 and 40 °C.

The calculated thermodynamic parameters for DPF soot and PAC are presented in Table 4. The Gibbs' Free Energy for all three metals is negative, which confirms the feasibility and spontaneous nature of the adsorption (Mohan and Singh 2002). Further, the negative values of enthalphy (H) indicate the exothermic nature of the adsorption process for both DPF

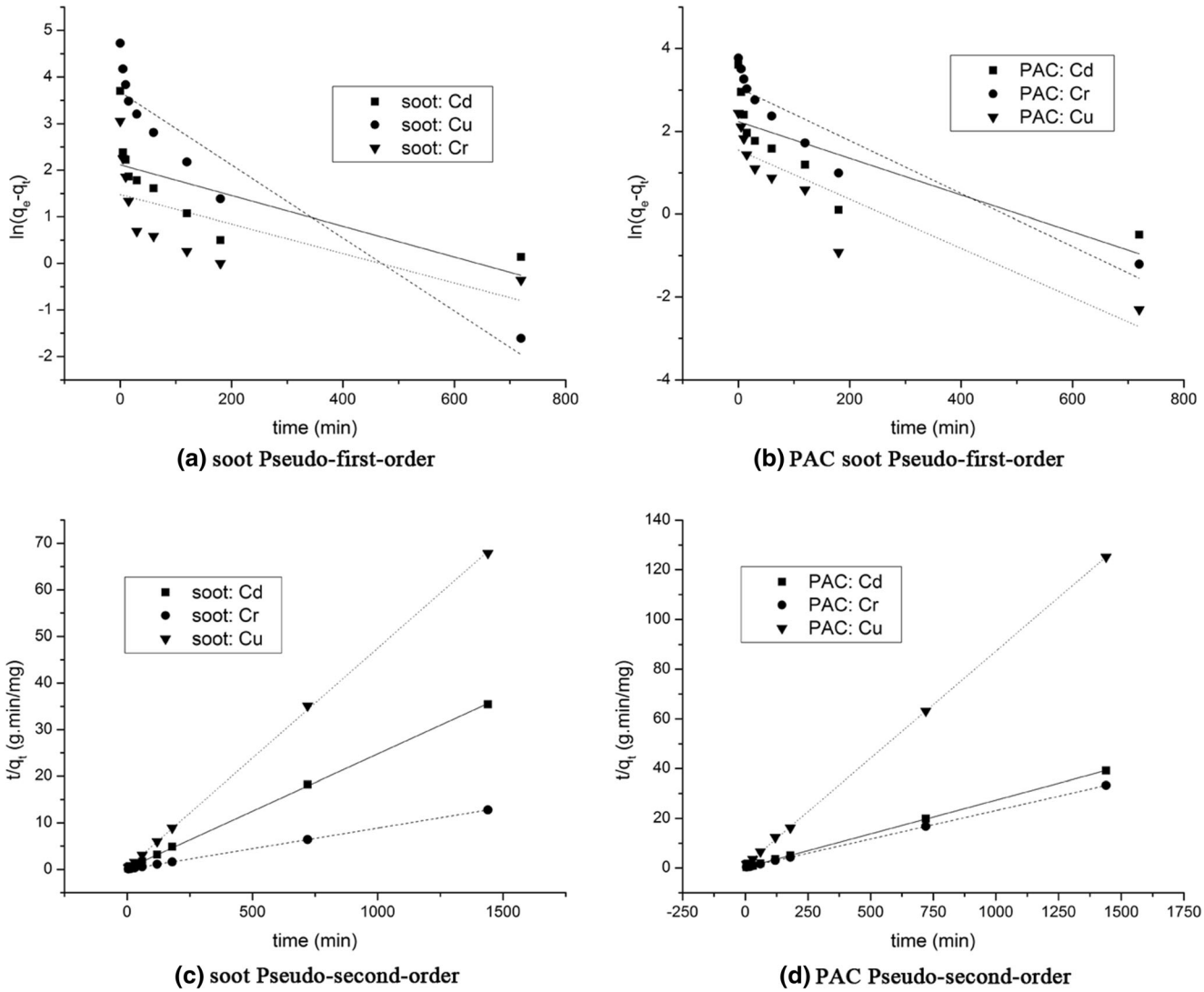

Fig. 12 Adsorption Kinetics at 25 °C: **a** and **b** corresponding to pseudo-first-order model, **c** and **d** corresponding to pseudo-second-order model

soot and PAC. Therefore, adsorption of Cd(II), Cu(II), and Cr(VI) will be inhibited by increased temperatures. This was confirmed by Sari and Tuzen (2009) and Sari et al. (2007) , who demonstrated the same phenomena for the inhibition of adsorption with increased temperatures for Cd(II) and Pb(II) onto biomass.

Binary adsorption isotherms

Adsorption in multi-component systems is more complicated than single compound systems due to competitive adsorption. The adsorption isotherms of binary contaminant systems of Cd(II)/Cr(VI), Cr(VI)/Cu(II), and Cd(II)/Cu(II) are presented

Table 8 Kinetic constants for adsorption of Cd(II), Cu(II), and Cr(VI)

	Soot				PAC			
	Pseudo-first-order		Pseudo-second-order		Pseudo-first-order		Pseudo-second-order	
	K_1	R^2	K_2	R^2	K_1	R^2	K_2	R^2
Cd(II)	0.0032	0.5627	0.004	0.998	0.0044	0.625	0.004	0.999
Cr(VI)	0.0078	0.9010	0.001	1.000	0.0064	0.888	0.001	1.000
Cu(II)	0.0032	0.4160	0.007	0.999	0.0059	0.805	0.005	0.999

in Fig. 11. The adsorption isotherms were obtained at 25 °C. For each binary system, 20 mg/L of Cr(VI) or Cu(II) was added to each solution ranging from 20 to 200 mg/L of Cd(II) or Cr(VI). For both DPF soot and PAC, the presence of 20 mg/L Cr(VI) or Cu(II) in the solution adversely affects the adsorption of Cd(II) and Cr(VI).

As reported in Table 5, the binary adsorption results are adequately fit by both Langmuir and Freundlich models. For Cd(II)/Cr(VI) and Cr(VI)/Cu(II), the Langmuir model fit the result slightly better than the Freundlich model as shown in Table 6. According to Table 7, the ultimate loadings for the single compound system is lower for Cd(II) and Cr(VI) compared to the binary system, specifically, the Cd(II) adsorption capacity reduced by almost half. And this data was slightly lower for Cr (VI), which means Cu(II) has weaker impaction on Cr(VI).

Adsorption kinetics

In order to understand the controlling mechanisms of the adsorption process such as mass transfer or chemical reactions, two kinetic models were tested, which were pseudo-first-order and pseudo-second-order. Based on the results presented in Fig. 12, the adsorption kinetics of Cd(II), Cu(II), and Cr(VI) are best modeled by pseudo-second-order. The regression coefficients for all metals tested herein support pseudo-second-order, as presented in Table 8. The pseudo-second-order model assumes that the initial adsorption rate is rapid followed by a slower adsorption rate, due to chemisorption mechanisms (Wang et al. 2011). Therefore, during the beginning of adsorption, the adsorption sites are open and metal ions interact rapidly with adsorbents due to high diffusion rates of metal ions attributed to the much higher concentration gradient between the bulk solution and adsorbent surface. However, the adsorption rate decreases sharply as diffusion slows due to lower concentration gradients across the adsorbent surface area (Amarasinghe and Williams 2007).

Conclusion

Porous carbon-based soot samples were recovered from a DPF and were utilized as an adsorbent in the present study. The equilibrium sorption of three metal ions, Cd(II), Cu(II), and Cr(VI) were appraised for both DPF soot and PAC. Herein, the authors appraised all three metals as single compound systems and as binary systems. The adsorption performance was appraised at both 25 and 40 °C. The surface microstructures of the DPF soot and PAC was characterized by SEM-EDS. The surface functional groups of both adsorbents were appraised by FTIR. The surface zeta potential of the carbon soot was studied to determine the isoelectric point.

Compared with activated carbon, DPF soot appears to possess more surface roughness and surface area as observed during SEM analysis. The EDS spectra revealed that the DPF soot possesses a similar chemical composition with commercial activated carbon. The FTIR results indicate that both the DPF soot and PAC are dominated by hydroxyl and carboxylic functional groups. Interestingly, the surface density of these functional groups appears higher for soot. Herein, both adsorbents possess a high surface acidity and low isoelectric point.

Results indicate that the adsorption of heavy metals by DPF soot and PAC occur through both electrostatic interaction and physical adsorption. The Gibb's free energies of adsorption were calculated to confirm the adsorption is exothermic and spontaneous for all three metals. The isotherm results for both single and binary systems were best fit by the monolayer model and Langmuir isotherm. The kinetic study demonstrated that the pseudo-second-order kinetic model best fits all three metal ions.

In sum, DPF soot is a viable adsorbent for the elimination of heavy metal pollution from aqueous systems. DPF soot could be a very low-cost adsorbent applied in this capacity; however, adoption requires overcoming the technical challenges of efficient recovery and purification.

Acknowledgements The authors would like to thank Hunsicker Emission Service, LLC, for providing the DPF soot for this work, which was recovered from a commercial vehicle's diesel particulate filter (DPF).

References

Amarasinghe BMWPK, Williams RA (2007) Tea waste as a low cost adsorbent for the removal of Cu and Pb from wastewater. Chem Eng J 132(1-3):299–309. https://doi.org/10.1016/j.cej.2007.01.016

Azizian S (2004) Kinetic models of sorption: a theoretical analysis. J Colloid Interface Sci 276(1):47–52. https://doi.org/10.1016/j.jcis.2004.03.048

Cho DW, Chon CM, Kim YJ, Jeon BH, Schwartz FW (2011) Adsorption of nitrate and Cr(VI) by cationic polymer modified granular activated carbon. Chem Eng J 175:298–305. https://doi.org/10.1016/j.cej.2011.09.108

Cheung CW, Porter JF, Mckay G (2000) Elovich equation and modified second order equation for sorption of cadmium ions onto bone char. J Chem Technol Biotechnol 75(11):963–970. https://doi.org/10.1002/1097-4660(200011)75:11<963::AID-JCTB302>3.0.CO;2-Z

Hamilton RS, Mansfield TA (1991) Airborne particulate elemental carbon: its sources, transport and contribution to dark smoke and soiling. Atmos Environ 25A:715–723

Jiang MQ, Jin XY, Lu XQ, Chen ZL (2010) Adsorption of Pb(II), Cd(II), Ni(II) and Cu(II) onto natural kaolinite clay. Desalination 252(1-3):33–39. https://doi.org/10.1016/j.desal.2009.11.005

Kyzas GZ, Deliyanni EA, Matis KA (2014) Graphene oxide and its application as an adsorbent for wastewater treatment. J Chem Technol Biotechnol 89(2):196–205. https://doi.org/10.1002/jctb.4220

Larkin P (2011) Infrared and Raman spectroscopy. Elsevier, 225 Wyman Street, Waltham, MA 02451, USA

Mellah A, Chegrouche S (1997) The removal of zinc from aqueous solution by natural bentonite. Water Res 31(3):621–629. https://doi.org/10.1016/S0043-1354(96)00294-1

Mahvi AH, Naghipour D, Vaezi F, Nazmara S (2005) Teawaste as an adsorbent for heavy metal removal from industrial wastewaters. Am J Appl Sci 2(1):372–375

Mishra PC, Patel RK (2009) Removal of lead and zinc ions from water by low cost adsorbents. J Hazard Mater 168(1):319–325. https://doi.org/10.1016/j.jhazmat.2009.02.026

Mohan D, Singh KP (2002) Single and multi-component adsorption of cadmium and zinc using activated carbon derived from bagasse an agricultural waste. Water Res 36(9):2304–2318. https://doi.org/10.1016/S0043-1354(01)00447-X

Okieimen FE, Okundia EU, Ogbeifun DE (1991) Sorption of cadmium and lead ions on modified groundnut (Arachis hypogea) husks. J Chem Technol Biotechnol 51:97–103

Qiu YP, Cheng HY, Xu C, Sheng GD (2008) Surface characteristics of crop residue derived black carbon and lead(II) adsorption. Water Res 42(3):567–574. https://doi.org/10.1016/j.watres.2007.07.051

Rao RAK, Kashifuddin M (2016) Adsorption studies of Cd(II) on ball clay: comparison with other natural clays. Arab J Chem 9:1233–1241

Street DG, Gupta S, Waldhoff ST, Wang MQ, Bond TC, Bo YJ (2001) Black carbon emissions in China. Atmos Environ 35(25):4281–4296. https://doi.org/10.1016/S1352-2310(01)00179-0

Salvat O, Marez P, Belot G (2000) Passenger car serial application of a particulate filter system on a common rail direct injection diesel engine. SAE International Paper No.: 2000-01-0473

Strelko V, Malik DJ, Streat M (2002) Characterization of the surface of oxidized carbon adsorbents. Carbon 40(1):95–104. https://doi.org/10.1016/S0008-6223(01)00082-3

Sappok A, Santiago M, Vianna T, Wong V (2009) Characteristics and effects of ash accumulation on diesel particulate filter performance: rapidly aged and field aged results. SAE International Paper No.: 2009-01-1086

Srivastava SK, Tyagi R, Pant N, Pal N (1989) Studies on the removal of some toxic metal ions. Part II removal of lead and cadmium by montmorillonite and kaolinite. Environ Technol Lett 10(3):275–282. https://doi.org/10.1080/09593338909384742

Sari A, Tuzen M (2009) Kinetic and equilibrium studies of biosorption of Pb(II) and cd(II) from aqueous solution by macrofungus (Amanita rubescens) biomass. J Hazard Mater 164(2-3):1004–1011. https://doi.org/10.1016/j.jhazmat.2008.09.002

Sari A, Tuzen M, Uluozlu OD, Soylak M (2007) Biosorption of Pb(II) and Ni(II) from aqueous solution by lichen (Cladonia furcata) biomass. Biochem Eng J 37(2):151–158. https://doi.org/10.1016/j.bej.2007.04.007

Sellaoui L, Dotto GL, Lamine AB, Erto A (2017) Interpretation of single and competitive adsorption of cadmium and zinc on activated carbon using monolayer and exclusive extended monolayer models. Environ Sci Pollut Res 24(24):19902–19908. https://doi.org/10.1007/s11356-017-9562-8

United States Environmental Protection Agency (USEPA) (2009) National primary drinking water regulations

Veli S, Alyuz B (2007) Adsorption of copper and zinc from aqueous solutions by using natural clay. J Hazard Mater 149(1):226–233. https://doi.org/10.1016/j.jhazmat.2007.04.109

Viidanoja J, Sillanpaa M, Laakia J, Kerminen VM, Hillamo R, Aarnio P, Koskentalo T (2002) Organic and black carbon in PM2.5 and PM10: 1 year of data from an urban site in Helsinki, Finland. Atmos Environ 36(19):3183–3193. https://doi.org/10.1016/S1352-2310(02)00205-4

Wang XS, Chen LF, Li FY, Chen KL, Wan WY, Tang YJ (2010) Removal of Cr(VI) with wheat residue derived black carbon: reaction mechanism and adsorption performance. J Hazard Mater 175(1-3):816–822. https://doi.org/10.1016/j.jhazmat.2009.10.082

Wang XS, Miao HH, He W, Shen HL (2011) Competitive adsorption of Pb(II), Cu(II), and Cd(II) ions on wheat residue derived black carbon. J Chem Eng Data 56(3):444–449. https://doi.org/10.1021/je101079w

Yang K, Fox JT, Hunsicker R (2016) Characterizing diesel particulate filter failure during commercial fleet use due to pinholes, melting, cracking and fouling. Emission Control Sci Technol 2(3):145–155

Zhou Q, Liu ZD, Liu Y, Jiang J, Xu RK (2016) Relative abundance of chemical forms of Cu(II) and Cd(II) on soybean roots as influenced by pH, cations and organic acids. Sci Rep 6(36373):1–9

Zhou DM, Wang YJ, Wang HW, Wang SQ, Cheng JM (2010) Surface modified nanoscale carbon black used as sorbents for Cu(II) and Cd(II). J Hazard Mater 174(1-3):34–39. https://doi.org/10.1016/j.jhazmat.2009.09.012